Volume 1 | Number 1 | Jan 2013 | Pages 1–100

Organic & Biomolecular Chemistry

www.rsc.org/obc

ROYAL SOCIETY OF CHEMISTRY

ROYAL SOCIETY OF CHEMISTRY

www.rsc.org/obc

Journal Name

Organic & Biomolecular Chemistry

ARTICLE TYPE

An ESIPT Fluorescent Probe Sensitive to Protein α-helix Structures

Nan Jiang, [a] **Chanli Yang,** [a] **Xiongwei Dong,** [a] **Xianglang Sun,** [a] **Dan Zhang,** [a] * **Changlin Liu** [a] *

5 **Abstract:** A large majority of membrane proteins have one or more transmemberane regions consisted of α-helices. Membrane protein levels are different from one type of cells to another, and the expression of membrane proteins is also altered from normal to diseased cells. For example, prostate cancer cells have been reported to have down regulated expression of membrane proteins including zinc transporters compared with prostate normal cells. These reports inspired us to design a fluorescence probe sensitive to
10 protein α-helical structures to discriminate individual prostate cancer cells from normal ones. A benzazole derivative (**1** in this study) was observed to emit strong fluorescence resulted from an excited-state intramolecular proton transfer (ESIPT) in protein α-helical environments. The intensity of ESIPT fluorescence of **1** was observed to be positively correlated with the α-helix contents of proteins. The molecular docking simulation suggested that it had low energy for the binding of **1** to proteins when the
15 binding sites were localized within the α-helical regions of protein via H-bonds. Furthermore, **1** was found to be localized in cell membranes through binding to transmembrane α-helical regions of membrane proteins and to be capable of probing a difference in the membrane protein α-helix contents between prostate normal and cancer cells by its changes in the ESIPT emission intensity. These results indicated that **1** could distinguish individual prostate cancer cells from normal ones, for the changes in the
20 ESIPT fluorescence intensity of **1** could reflect the regulation in expression of the membrane proteins including zinc transporters. The recognition strategy of individual prostate cancer cells might contribute to the early diagnosis approaches of prostate cancer.

Introduction

25 Excited-state intramolecular proton transfer (ESIPT) is a reaction that occurs in certain fluorescent molecules in an excited state.[1] In the ground state, an ESIPT molecule exists in enol tautomer state (E); upon irradiation with light, the molecule is driven to excited state (E*) and emits fluorescence (called as N* emission)
30 in a short wavelength range. When the excited molecule localizes in a suitable microenvironment, a proton can be transferred from its H-bonding donor group to its H-bonding acceptor group to generate the corresponding keto tautomer (K*). The fluorescent molecule in the excited keto state emits fluorescence (called as
35 T* emission) with a large Stokes shift in a longer wavelength range relative to the N* emission (Scheme 1).[2] The ESIPT molecules that exhibit characteristic two-band fluorescence spectra in suitable microenvironments can act as a fluorescence probe to obtain insights into some biological processes.[3–5]
40 Demchenko's group used a derivative of the most typical ESIPT fluorescent molecules, 3-hydroxyflavone, as a site-sensitive fluorescence label for α-crystallin, and proposed that this labelling method might offer a possibility to study structures, dynamics and intermolecular interactions of the labelled
45 proteins.[6–9] Stefani's group reported the use of the benzazole
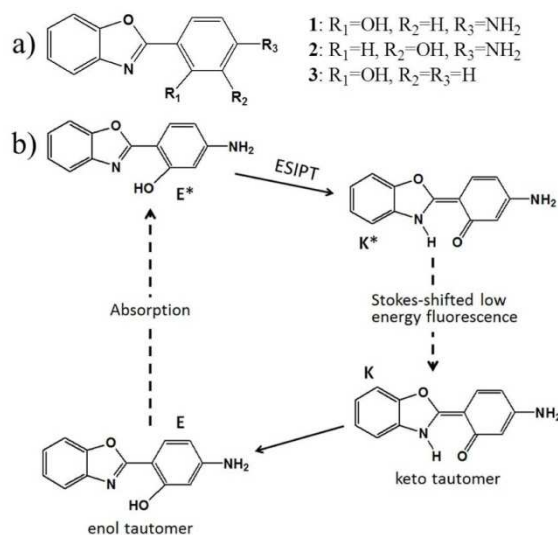
Scheme 1 a) Structures of **1**–**3**. b) ESIPT reaction in **1**. E* and K* represented the excited enol and keto tautomers of 1, respectively.

50 derivatives to stain *Candida albicans* ATCC 10231 cells and characterize nanocapsule polymeric walls, as well as to probe rice protein and bovine serum albumin (BSA) in solutions, but the

detailed mechanisms remained to be explored.[10–14]

A large majority of membrane proteins have one or more transmemberane regions consisted of α-helices. Membrane protein levels are different from one type of cells to another, and the expression of membrane proteins is also altered from normal to diseased cells.[15] For example, in the development of prostate cancer, the intracellular mobile zinc ion levels are notably decreased,[16–19] along with the downregulation in expression of *Zip*-family proteins (hZip1, hZip2, hZip3) which have been reported to be responsible for the accumulation of zinc in prostate cells.[20–22] The zinc transporters including *hZip1–3* (UniProt, Q9NY26, Q9NP94 and Q9BRY0) have eight potential transmembrane α-helices.[23] Obviously, the downregulation expression of zinc transporters can lead to decrease in protein α-helix contents in prostate cancer cell membranes. Therefore, the changes in α-helix contents in cell membranes might become a candidate biomarker for recognition of individual prostate cancer cells, given that the expression of membrane proteins other than zinc transporters is not pronouncedly changed in the transformation of prostate normal cells to cancer cells.

In this study, we found an ESIPT molecule **1** (5-amino-2-benzooxazol-2-yl-phenol, a derivative of 2-(2'-hydroxyphenyl) benzazole) that emitted a strong ESIPT fluorescence in both some organic solvents and proteins with a high α-helix content (Scheme 1). The strong ESIPT fluorescence was brought about by the biding of **1** to proteins with a high α-helix content. The sensitivity of **1**'s ESIPT fluorescence to protein α-helix structures could be used to probe changes in the protein α-helix content in prostate cell membranes. Because the changes in the α-helix content could reflect the expression of membrane proteins, individual prostate cancer cells could be distinguished from normal cells by utilizing of the changes in the **1**'s ESIPT fluorescence intensity.

Results and Discussion

ESIPT fluorescence in organic solvents

Three benzoxazole molecules **1–3** (Scheme 1) were prepared and characterized according to the previously reported synthesis approach (See Supporting Information Fig. S1 for detailed data).[10,24] Compared to **2**, it was easy for **1** and **3** to undergo ESIPT reaction due to the suitable distance between their H-bonding acceptor N atoms and OH groups. In order to examine alterations in the ESIPT property of **1** and **3** in different microenvironments, three organic solvents, the protic solvent ethanol and aprotic solvents chloroform and dichloromethane, were chosen in light of their polarity and H-bonding ability.[25] Both polarity and H-bond acceptor ability decreased in the order of ethanol > dichloromethane > chloroform.
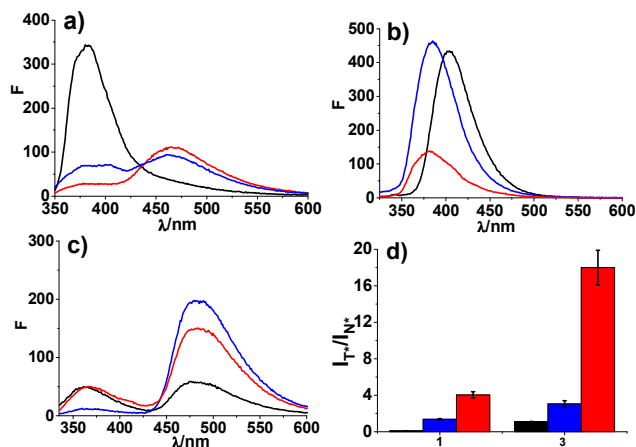

Fig. 1 Fluorescence spectra of 8 μM **1** (a, λex = 335 nm), **2** (b, λex = 310 nm) and **3** (c, λex = 320 nm) in EtOH (—), CH_2Cl_2 (—), $CHCl_3$ (—) at 25°C, respectively. d) Relative emission intensity ratios of T* to N* bands of **1** ($I_{460\,nm}/I_{390\,nm}$) and **3** ($I_{483\,nm}/I_{367\,nm}$) in these three solvents.

Whether **1–3** underwent ESITP reaction was obvious from their fluorescence spectra in the selected solvents (Fig. 1a–c). Two well-separated intensive fluorescence peaks were observed for **1** in both chloroform and dichloromethane and for **3** in these three solvents (Fig. 1a, c), being corresponding respectively to enol (N*) and keto tautomer (T*) emissions, as previously reported,[10,26] but **2** produced only the normal emission under the conditions tested (Fig. 1b). These results indicated that **1** and **3** underwent an ESIPT reaction, but **2** did not, in the solvents. In order to confirm occurrence of the ESIPT reactions in **1** and **3**, the intensity ratios of T* to N* emission (I_{T*}/I_{N*}) were determined (Fig. 1d). Obviously, the I_{T*}/I_{N*} ratios were significantly reduced with an increase in the H-bonding ability of solvents, and greater in chloroform than in both dichloromethane and ethanol. This fact indicated that it was much easier to undergo the ESIPT process in the aprotic solvents with no H-bonding ability, because the H-bonds between a fluorescent molecule and a solvent molecule could interferes in the formation of keto tautomers. That could lead to disappearance of the ESIPT emission, which also occurred when **1** was in ethanol (Fig. 1a). Moreover, the hydroxyl group in the ortho-position of benzoxazolyl in **1** and **3** was essential for ESIPT. In addition, the electron-donating group NH_2 in **1** could enhance electron density on the OH group and reduce the intramolecular proton transfer, which resulted in the intensity of the ESIPT emission or the I_{T*}/I_{N*} ratio of **1** being much less than that of **3** under the conditions tested.

ESIPT fluorescence in protein α-helix environments

The analogues of **1–3** were reported to emit ESIPT fluorescence at ~460 nm in BSA solutions.[10] The hydrophobic and low polar sites within a protein were similar to the environments that comprise the organic solvents with low polarity, and should facilitate the ESIPT emission. Therefore, fluorescence spectra were utilized to examine whether **1–3** underwent ESIPT reaction in the solutions of the proteins containing varied α-helix contents. We selected four proteins, BSA, human serum albumin (HSA), lysozyme and trypsin, and their α-helix contents were listed in Table 1. The fluorescence spectra of **1–3** were first measured in

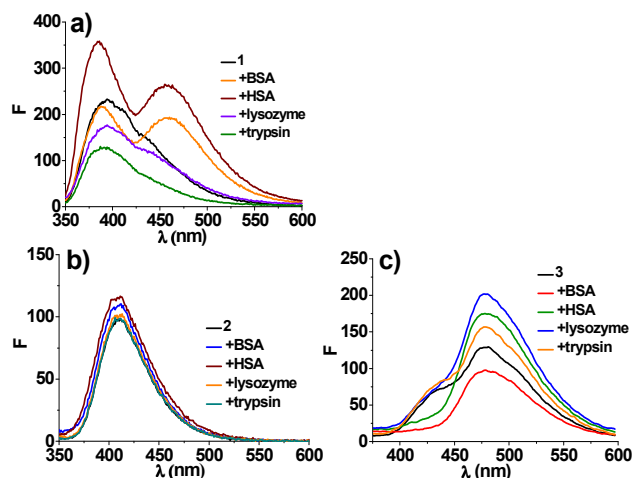the buffer used as control. The results showed that the normal

Fig. 2 a) Fluorescence spectra of 8 μM **1** (λex = 335 nm) in the presence
5 of 32 μM BSA, HSA, lysozyme and trypsin, respectively. b) Fluorescence
spectra of 0.5 μM **2** (λex = 310 nm) in the presence of 2 μM BSA, HSA,
lysozyme and trypsin, respectively. c) Fluorescence spectra of 8 μM **3**
(λex = 320 nm) in the presence of 32 μM BSA, HSA, lysozyme and
trypsin, respectively. All fluorescence experiments were performed in 100
10   mM Tris-HCl buffer (pH 7.4, 150 mM NaCl) at 25°C.

fluorescence band at ∼ 400 nm arose from the enol tautomers of
excited **1** and **2,** whereas the fluorescence at ∼ 485 nm was the
ESIPT emissions that arose from the keto tautomers of excited **3**
(Fig. 2a–c). These results indicated that only the fluorescence
15 from either enol or keto tautomer could be observed in the buffer.
Then, **1** was observed to produce a well-separated fluorescence
band at ∼ 460 nm in BSA and HSA solutions in addition to the
normal band at ∼ 390 nm, but not in the other two protein
solutions (Fig. 2a). However, **2** and **3** emitted only either strong
20 enol or keto tautomer fluorescence in all the four protein
solutions under the conditions tested, as observed in the buffer
(Fig. 2b, c). These results revealed that **1** underwent ESIPT
reaction in the proteins which had high α-helix contents (66% for
BSA and 71 % for HSA), suggesting that the ESIPT fluorescence
25 of **1** might be notably sensitive to protein α-helical structures.

In order to prove the sensitivity of **1**'s ESIPT emission to
protein α-helical structures, the effects of BSA concentrations,
temperature, and protein denaturing agents on fluorescence
spectra of **1** were examined respectively. Firstly, the fluorescence
30 spectra were recorded at the fixed **1** and varied BSA
concentrations. The results showed that the I_{T*}/I_{N*} ratios were
significantly increased with increasing BSA to **1** molar ratios (Fig.
3a, b). Then, the intensity of both T* and N* emissions from the
solutions, which contained BSA and **1** at a given concentration,
35 was observed to be reduced with temperature rise (Fig. 3c, d), so
were the I_{T*}/I_{N*} ratios (Fig. 3d). These results could be attributed
to loss of the natural α-helix structures in BSA caused by heating.
To rule out the possibility that the temperature sensitivity of the
ESIPT emission was an artifact caused by heating, the
40 fluorescence spectra of **1** in the absence of BSA were measured at
the given temperature range. As expected, only the normal
emission was observed for **1** under the conditions tested (Fig. S3).
Moreover, the intensity of this emission was reduced with
heating, and the reduction extent was similar to that observed in
45 the presence of BSA. These facts showed that the ESITP

emission of **1** was positively correlated with the content of
ordered α-helix structures in a protein. As a result, the
combination of the BSA concentration and temperature
experiments suggested that the ESITP emission intensity of **1** was
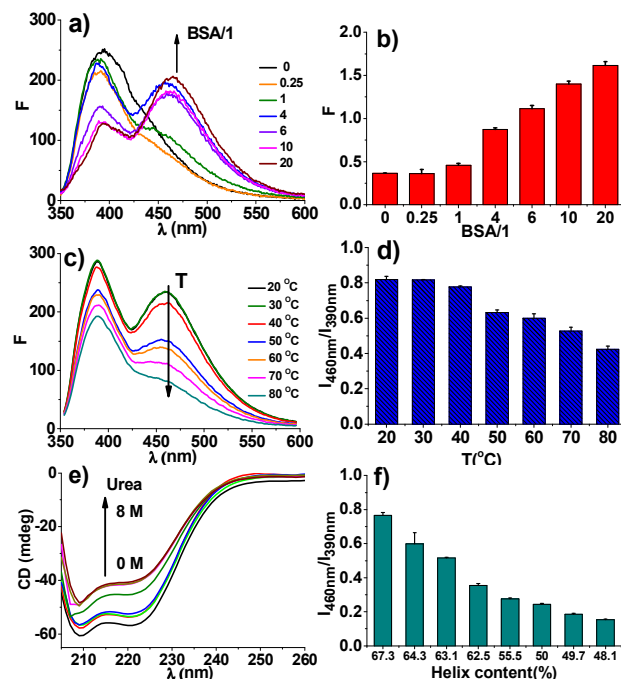50 sensitive to the α-helix content in a protein.

Fig. 3 a) Fluorescence spectra of 8 μM **1** upon increased addition of BSA
55 (0–160 μM). b) The effect of BSA/**1** mole ratios on T*/N* emission
intensity ratios (I_{460nm}/I_{390nm}) of **1**, calculated utilizing the fluorescence
spectra in a). c) Fluorescence spectra of 8 μM 1 in the presence of 32 μM
BSA in the temperature range of 20–80 °C. d) The effect of temperature
on I_{460nm}/I_{390nm} ratios of **1**, calculated utilizing the fluorescence spectra in
60 c). e) CD spectra of 32 μM BSA exposed to 0–8 M urea. f) I_{460nm}/I_{390nm}
ratios of 8 μM **1** was reduced with decreasing α-helix contents of BSA
exposed to 0–8 M urea. The α-helix contents of BSA exposed to 0–8 M
urea were calculated based on the CD spectra in e). All fluorescence
experiments were performed in 100 mM Tris-HCl buffer (pH 7.4, 150
65 mM NaCl) at 25°C. The error bars were the results from at least three
parallel measurements.

To further confirm the correlation of the ESITP emission
intensity of **1** with the α-helix content in a protein, the α-helical
protein BSA was treated with varied urea concentrations.
70 Because urea could disrupt the secondary and tertiary structures
of proteins, the α-helix content in BSA would be reduced with
increasing urea concentrations[27,28]. The treatment with 0–8 M
urea led to the reduction of α-helix content from 67.3% to 48.1%
in 32 μM BSA, as demonstrated by circular dichroism (CD)
75 spectra (Fig. 3e). With reduction of the α-helix content in BSA,
the I_{T*}/I_{N*} ratios of **1** were observed to significantly decrease
from 0.76 to 0.15 (Fig. 3f). The result of the protein denaturing
experiment, together with the results described above, proved that
the ESIPT emission intensity of **1** was dominated by the α-helix
80 content in a protein.

The sensitivity of the ESIPT fluorescence of **1** to the proteins
with high α-helix contents could be understood in light of the
protein hydrophobic sites which were consisted of α-helices. On
the one hand, if **1** could be localized in a suitable site within an α-
85 helical protein, it would be possible to form H-bonds between its

NH$_2$ group and the amide groups (either CO or NH) on protein α-

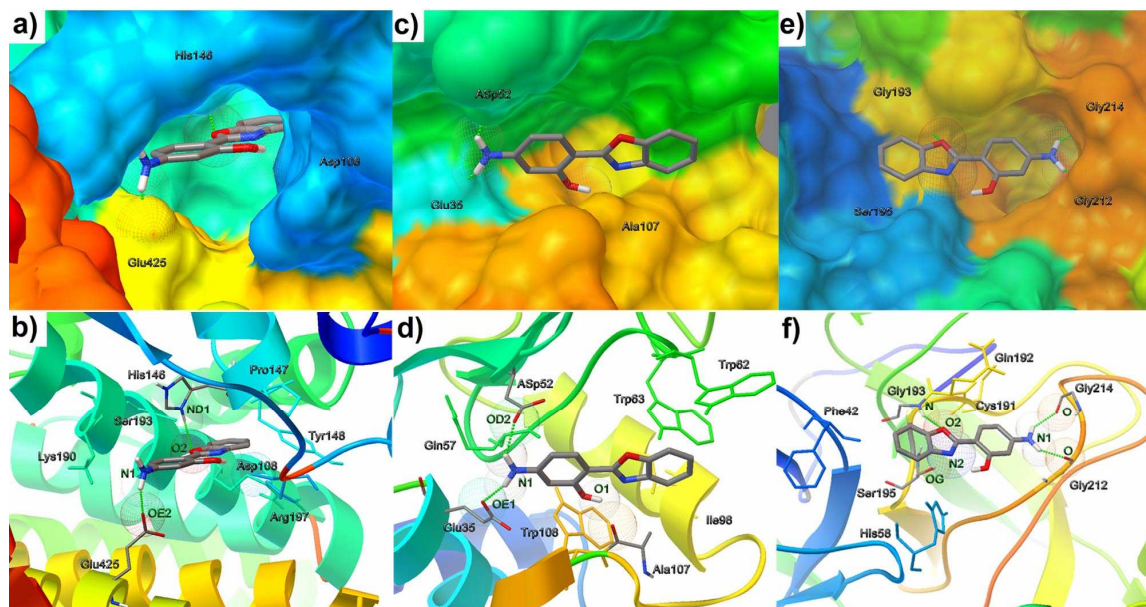helices. The intermolecular H-bonds could reduce the electron-

Fig. 4 The interactions between **1** and protein molecules visualized by molecular docking simulation. Here, **1** was represented as stick models; C: grey, N: blue, O: red. Up, the hydrophobic cavities in HSA (a), lysozyme (c) and trypsin (e) for **1** binding were displayed by molecular surface models. The residues involved in the H-bonds between **1** and HSA (b), lysozyme (d) or trypsin (f) were highlighted. Bottom, the proposed H-bonds were shown as green dashed lines. The residues involved in the interactions between **1** and protein molecules were indicated, and the fragments of protein secondary structures were showed by different colours.

donating ability of the NH$_2$ group and weaken the O–H bond in **1**. Obviously, this was in favor of formation of the intramolecular O–H···N H-bond in **1**, which resulted in readier proton transfer from the OH group to benzoxazolyl N atom on **1** in the protein-bound state than in the protein-free state. Therefore, the strong fluorescence emission caused by the ESIPT reaction in **1** could be observed in the BSA- or HSA-containing medium. In the contrast, no new emission was found for **2** and **3** in the BSA solution (Figure 2b, c) because of lack of the intra- or inter-molecular H-bonds.

Obviously, it was difficult to form the intramolecular H-bond in **2** owing to the large separation between its benzoxazolyl N atom and OH group despite it was in favor of the formation of intermolecular H-bonds between **2** and the proteins. However, it was ready for **3** to form the intramolecular H-bond in both the presence and the absence of BSA because of lack of the NH$_2$ group, leading to the occurrence of **3** in the keto form even in the absence of proteins. Therefore, **2** and **3** could not undergo the ESIPT reaction similar to that in **1** when exposed to BSA and HSA. In addition, the differences in fluorescence spectra between **1** and **3** revealed an essential role of the NH$_2$ group in the ESIPT fluorescence of **1** in the protein-bound state. On the other hand, the ordered hydrophobic sites in a protein which were consisted of α-helices can offer a low polar microenvironment for fluorescence emission. Thus, N* and T* bands, as well as the I_{T*}/I_{N*} ratio of **1** were observed to be enhanced in the BSA and BSA solution compared with the other two proteins with low α-

helix contents (41% for lysozyme and 10% for trypsin) (Fig. 2a). As a result, it was reasonable to conclude that the ESIPT fluorescence of **1** could be ascribed to the suitable localization of **1** in the α-helical environments within a protein likely via the intermolecular H-bonds between the NH$_2$ group on **1** and an amide group in the protein.

Molecular docking into α-helical sites in a protein

In order to support the hypothesis that **1** could associate with the α-helical proteins BSA and HSA via the intermolecular H-bonds between the NH$_2$ or OH group on **1** and amide groups in the proteins, molecular docking simulation was carried out by using AutoDock program (version 4.2.0)[29,30] based on the protein structural data. The results delineated above indicated that the ESIPT fluorescence of **1** was sensitive to α-helix structures in BSA and HSA. HSA was selected for the molecular docking with **1** as the structural data of HSA are available in Protein Data Bank (PDB), and HSA is homologous to BSA. The interactions between **1** and lysozyme or trypsin were also simulated for comparison. The **1**-bound hydrophobic sites in the proteins were visualized by molecular surface models (Fig. 4a, c, e), indicating that the shapes of the sites for **1** binding were different from one type of protein structures to another type. This result highlighted that the α-helical sites or sites rich in α-helices were the appropriate ones for **1** binding in proteins.

The docking calculation showed that binding energy of **1** to HSA (−5.33 kcal/mol) was lower than those of **1** to both trypsin

ARTICLE TYPE

Table 1 The simulation data for molecular docking of **1** into the proteins selected.

| Proteins (PDB)	Helix content (%)	Distance of intermolecular hydrogen bonds (Å)		Angle (°)	Binding energy (Kcal/mol)
HSA (1BM0)	71[31]	N_1-H----OE_2 (Glu425) O_2----H-ND_1 (His146)	2.678 2.989	139.4751 48.451	−5.33
Lysozyme (3RT5)	41	N_1-H----OE_1 (Glu35) N_1-H----OD_2 (ASp52)	3.018 2.921	158.2631 36.161	−5.1
Trypsin (3ATK)	10[32]	N_1-H----O (Gly214) N_1-H----O (Gly212) O_2-----H-N (Gly193)	3.103 3.077 3.167	140.6591 46.58315 2.173	−4.03
Potassium ion channel (1BL8)	67[33]	N_1-H----O (Thr74(A))	2.664	142.308	−5.83
Glucose transporter (4GBZ)	76[34]	--		--	−5.35
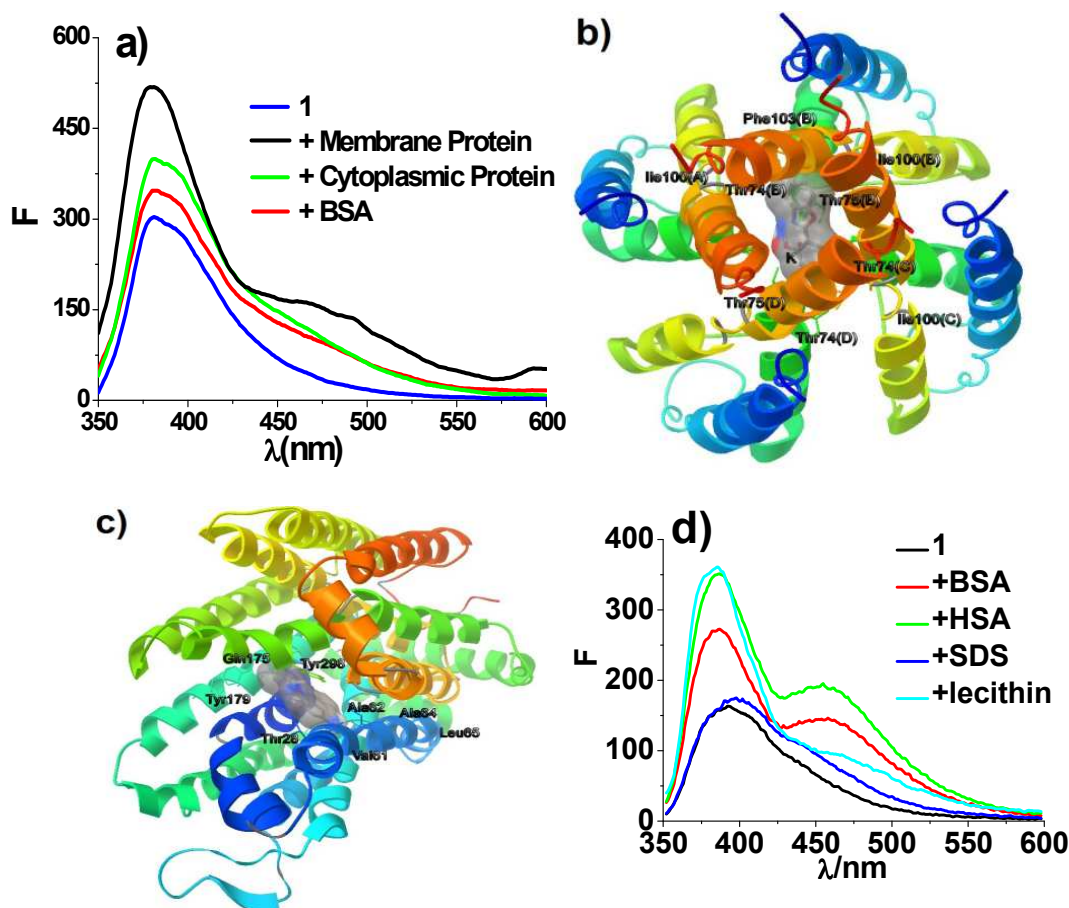
Fig. 5 a) Fluorescence spectra of **1** in the presence of membrane proteins, cytosol proteins and BSA, respectively. The membrane and cytosol proteins were extracted from Hela cells. The concentrations of samples were 0.2 mg protein/mL. b, c) H-bonds, residues, and secondary structures involved in interactions between **1** and a potassium channel b) or glucose transporter c). The binding modes between **1** and the membrane proteins were visualized by the molecular docking simulation. d) Fluorescence spectra of 8 μM **1** (λex = 335 nm) in the presence of 32 μM BSA, HSA, 320 μM SDS, and 0.1% lecithin (0.01 g lecithin in 10 mL Tris-HCl buffer) respectively. All fluorescence experiments were performed in 100 mM Tris-HCl buffer (pH 7.4, 150 mM NaCl) at 25°C.

ARTICLE TYPE

(−5.1 kcal/mol) and lysozyme (−4.03 kcal/mol) (Table 1). The data also demonstrated that the α-helices played a key role in the binding. As it was indicated by the docking, the binding energy was mainly dominated by the intermolecular energy which was 5 dependent on H-bonds between **1** and the proteins (Fig. 4b, d, f). Therefore, the differences in the H-bonding strength and modes could underlie the change in the binding energy. It was clear from Fig. 4b, d, f that the H-bonds could form only between the NH$_2$ group on **1** and the proteins, and both the benzoxazolyl N atom 10 and OH group on **1** were not involved in formation of the intermolecular H-bonds, as anticipated. Therefore, the intramolecular O–H···N H-bond in **1** was not affected (Scheme 1). On the basis of the H-bond length data (Table 1), the H-bonding strength between the NH$_2$ group on **1** and the 15 corresponding residues was decreased with a fall in the α-helix contents in the tested proteins. Obviously, the intermolecular strong H-bonds were in favor of decreasing the electron density of the OH group on **1**, and it thereby promoted the intramolecular proton transfer in **1**. As a result, a significant ESIPT reaction 20 occurred in the HSA-bound form of **1**, that is, the stronger ESIPT emission could be observed for HSA exposure of **1** compared with lysozyme or trypsin exposure. In addition, a comparison in the H-bonding modes between HSA and lysozyme (Fig. 4b, d) suggested that the arrangements of α-helices in proteins could 25 also play a role in **1** binding. The parallel and near parallel distributions of α-helices might be in favor of **1** association with the proteins. Taken together with those obtained from the fluorescence experiments performed above, it was reasonable to conclude that the ESIPT fluorescence of **1**–**3** in protein α-helical 30 environments was dependent not only on the intramolecular position of the OH group on **1**, but also on the localization within protein molecules of the NH$_2$ group on **1** bound to α-helical sites via H-bonds.

Sensitivity of 1's ESIPT fluorescence to intracellular α-helical 35 proteins

Although intracellular proteins have varied α-helix contents with protein structure types, the transmembrane regions in a large majority of membrane proteins are consisted mainly of α-helices.[35–37] This stimulated us to examine fluorescence spectra of 40 **1** in the membrane protein solutions. We extracted respectively membrane and cytosol proteins (0.2 mg/mL) from Hela cells by cell lysis to perform this examination. The membrane proteins in samples were consisted of cell and plasma membrane proteins. The fluorescence spectra of **1** in the samples, as well as in BSA 45 solution (0.2 mg/mL), were determined under identical conditions. Compared with **1** in the buffer tested, any significant fluorescence emission was not observed in 425−550 nm for **1** exposed to the cytosol protein and BSA (Fig. 5a) at the given concentrations. Obviously, **1** can not emit observable 50 fluorescence in 425−550 nm in the solution of low BSA concentrations because of its BSA concentration-dependent ESIPT reaction (Fig. 3a, b). Meanwhile, this result also indicated

that an ESIPT reaction was not pronounced in **1** exposed to the cytosol proteins. However, when treated with the membrane 55 protein solution, **1** was observed to emit noticeable fluorescence in 425−550 nm (Fig. 5a), demonstrating that an ESIPT reaction was remarkable in **1** with membrane protein environments. Furthermore, because the ESIPT emission of **1** was positively correlated with α-helix contents in proteins, as indicated above, 60 the noticeable ESIPT reaction in **1** suggested that the α-helix contents in membrane proteins was much higher than those in the cytosol proteins at the given concentration as expected. In addition, the normal emission of **1** was considerably enhanced by the treatment with the membrane proteins compared to that with 65 the cytosol proteins (Fig. 5a), indicating that the α-helical motifs in membrane proteins could create an ordered environment that facilitated the normal fluorescence emission of **1**. In contrast, the effects of both lipids and detergents on **1**'s ESIPT fluorescence were examined to rule out the possibility that the hydrophobic 70 environments created by both of them were in favor of **1**'s ESIPT fluorescence. Compared with BSA and HSA proteins, lecithin (lipid) and SDS (detergents) could not make **1** undergo ESIPT (Fig. 5d) reaction. As a result, it was concluded that fluorescence of **1** was a sensitive probe to the membrane proteins with high α-75 helical contents.

The enhanced ESIPT and normal fluorescence of **1** implied an interaction between **1** and α-helical regions in membrane proteins. To understand this interaction, the molecular docking simulation of **1** with typical membrane protein molecules was 80 carried out by using the same docking approach as above. A potassium ion channel and a glucose transporter were selected for the docking simulation because these two most abundant proteins in membranes have the transmembrane regions that were completely consisted of α-helices, as demonstrated by x-ray 85 structures.[33,34] On the one hand, the docking data (Table 1) showed that the binding energies of **1** to this pair of membrane proteins were −5.83 and −5.35 Kcal/mol respectively, which were lower than that of **1** to HSA. On the other hand, the results indicated that the binding sites of **1** did localize within α-helical 90 regions in membrane proteins, and **1** had a similar binding mode in the α-helical regions (Fig. 5b, c) to that in HSA (Fig. 4a, b). The binding mode was controlled by the H-bond between the NH$_2$ group on **1** and the corresponding residues on α-helices. The strong H-bonds of **1** to membrane proteins, as indicated by bond 95 length data (Table 1), facilitated the occurrence of an ESIPT reaction in **1** by reducing the electron density on its OH group. Thus, the H-bond between the NH$_2$ and α-helices underlaid the
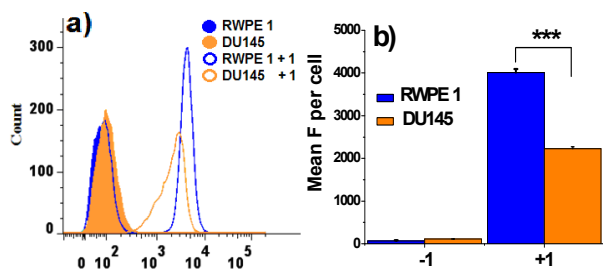
Fig. 6 a) A representative flow cytometry raw histogram for fluorescence intensity of **1**. b) Mean fluorescence intensity of 4 μM **1** per RWPE 1 or DU145 cell after incubation for 1 h. Results were representative of at least five independent experiments. ***P < 0.001.

observed ESIPT emission of **1** in membrane proteins. In addition, the hydrophobic and ordered binding sites comprising α-helices were in favor of enhancing the normal fluorescence of **1** in membrane proteins. As a consequence, a combination of the molecular docking data and fluorescence determination revealed that the fluorescence intensity of **1** was a sensitive probe to alterations of α-helix contents in membrane proteins.

Response of 1's fluorescence to membrane proteins in living prostate cells

The observations delineated above inspired us to examine whether the fluorescence of **1** could be changed with protein α-helix contents in living prostate cells. In order to conveniently perform this examination, prostate normal (RWPE 1) and cancer cell (DU145) lines were selected, for a notable difference was reported in expression of the *Zip* family membrane proteins between these two types of cells[38] and the different expression levels of *Zip* family proteins might be shown by the interactions with **1**. In light of the reported results,[23] the *Zip* family proteins (h*Zip*1, h*Zip*2, and h*Zip*3) all have eight potential transmembrane α-helices. To observe the differences in fluorescence of the intracellular **1** between prostate normal and cancer cells, the fluorescence intensity (excited at 375 nm) from the cells exposed to 4 μM **1** under the conditions tested was quantified by collecting Hochest-blue channel signals with a flow cytometry, because the ESIPT reaction in the membrane protein-bound **1** led to blue fluorescence (maximum at ~ 460 nm, Fig. 2a). The cytometric data showed that the mean fluorescence intensity per DU145 cell (at least 5 parallel assays) was reduced ~ 50% relative to that from per RWPE 1 cell after exposure to **1** (Fig. 6). Obviously, this result, which was well-consistent with that obtained by using the extracted membrane proteins provided by living cell lysis, provided a line of evidences to support the previously reported observation that expression of the membrane proteins including zinc transporters were significantly downregulated in the prostate cancer cells DU145. This indicated that the change in ESIPT fluorescence intensity of **1** was a measure of alteration in expression of the membrane proteins in cells.

Distinguishing individual prostate cancer cells from normal ones

The observations above performed showed a significant difference in the fluorescence intensity of **1** between the stained RWPE 1 and DU145 cells, indicating that **1** might provide a novel method to distinguish individual prostate cancer cells from
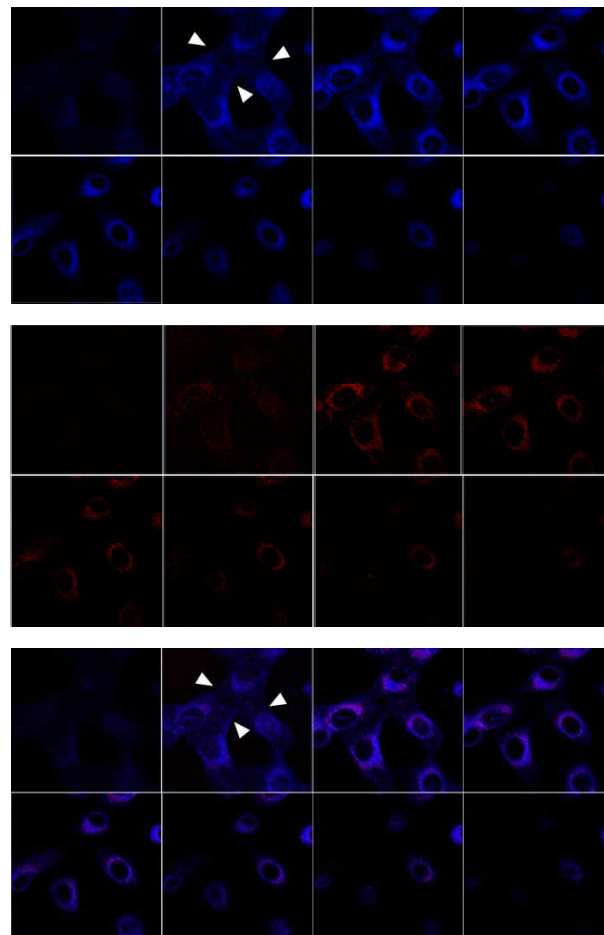

Fig. 7 Z-axis two-dimensional confocal fluorescence images for scanning analysis of 4 μM **1** and 40 nM ER-Red in RWPE 1 cells. Single optical sections (at 1.5-μm steps) were selected at various distances from the bottom surface were shown. Upper: Collected the fluorescence signal from 430 to 490 nm emitted only by **1**; Middle: Collected the fluorescence signal from 581 to 641 nm emitted only by ER-Red; Bottom: Merged between Upper and Middle. "▽" indicated the cell membrane.

normal ones by fluorescent imaging the changes in membrane protein levels. In order to use the ESIPT fluorescence of **1** to recognize prostate cancer cells, localization of **1** in prostate cells was examined by two-photon confocal microscopy. Firstly, the intracellular distribution of **1** was observed by co-staining the prostate normal cells RWPE 1 with **1** and ER-Tracker Red dye (ER-Red). ER-Red is a fluorescence dye that is capable of visualizing endoplasmic reticulum (ER) via specific binding to sulphonylurea receptor (SUR) subtypes in ER.[39] The cells were imaged by two-photon excitation at 800 nm for **1** and single-photon excitation at 561 nm for ER-Red respectively, after exposed to these two fluorescent molecules under the conditions tested. The fluorescence signals from 430 to 490 nm were acquired for imaging to utilize the ESIPT emission from the membrane protein-bound **1**. The Z-axis scanning images showed that **1** was localized in ER like ER-Red, as illustrated by the blue and red areas in (Fig. 7, middle), but it also distributed in cell membrane unlike ER-Red, as demonstrated by the clear cell profiles (Fig. 7, upper). Moreover, **1** also appeared in other cytosol membrane in addition to ER, as indicated by merged images with ER-Red (Fig. 7, bottom). In addition, the
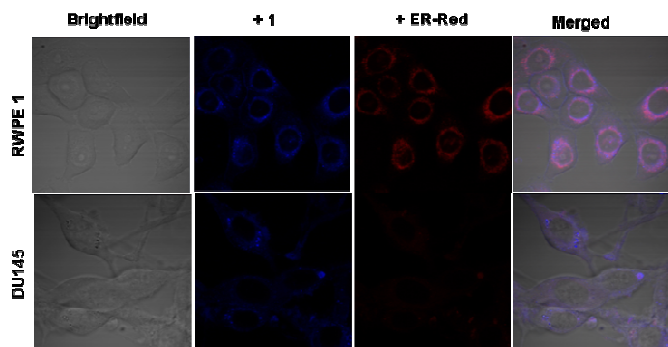
Fig. 8 Confocal images of cell lines RWPE 1 and DU145, after treated with 4 μM **1**, followed by staining with 40 nM ER-Red.

observations with the artificial phospholipid membrane indicated that **1** can retard in and penetrate the artificial membrane, but the retention in the membrane could not lead to the observable ESIPT fluorescence (Fig. 5, d).[40] As a result, these results allowed us to conclude that **1** visualizes cell and cytoplasmic membranes via binding to membrane proteins, not via retention in membranes.

Then, the cell lines RWPE 1 and DU145, which have a notable difference in the expression of membrane proteins including *Zip*-family proteins, were exposed to 4 μM **1** under identical conditions. The obtained confocal images showed that the blue fluorescence in each RWPE 1 cell was much brighter than that in DU145 cells (Fig. 8). The results, which were in agreement with those of flow cytometry, indicated that the α-helix contents were decreased in the order of RWPE 1 > DU145 in light of the ESIPT emission intensity of **1**. This fact revealed that **1** was a promising fluorescent probe to distinguish individual prostate cancer cells from normal ones.

Experimental Section

General methods

All reagents were purchased from commercial sources and used as received unless stated otherwise. The benzoxazole molecules **1–3** were prepared and characterized according to the reported synthesis program (See Fig. S1 in Supporting Information).[10,24] All solutions and buffers were prepared using Millipore-purified water. UV-visible absorption spectra were measured with a SPECORD 210 Ultra-visible spectrophotometer (Analytic Jena AG). ^{1}H and ^{13}C NMR spectra were recorded on a Varian VXR 500 spectrometer.

Fluorescence experiments

All fluorescence measurements were carried out with a Cary Eclipse fluorescence spectrophotometer (Varian, USA) at 25°C. For studies of **1–3** under different conditions, fluorescence spectra of **1–3** were recorded respectively in 100 mM Tris-HCl buffers (pH 7.4, 150 mM NaCl) containing 32 μM BSA (Roche), HSA (Sigma), lysozyme or trypsin (Biosharp) in the emission wavelength range of 350–600 nm (λex = 335 nm, 1 cm of cell length). These proteins have varied α-helix contents (from 71% to 10%, Table 1). To examine effects of protein/**1** ratios and temperature on fluorescence of **1**, fluorescence spectra of **1** were acquired for 0–160 μM BSA-containing samples or for 32 μM BSA treated for 10 min by heating in temperature range of 20–80 °C. To estimate effects of protein denaturing reagents on

fluorescence of **1**, fluorescence spectra of **1** were recorded for 32 μM BSA exposed to 0–8 M urea (Sigma) for 40 min at 37 °C. When examined the fluorescence response to membrane proteins, **1** was added respectively into membrane and cytosol proteins (0.2 mg protein/mL) extracted from Hela cells and its fluorescence spectra were recorded under the same conditions. For all fluorescence studies of **1**, fluorescence spectra of all samples were recorded following incubation for 5 min at 37 °C unless stated otherwise.

Evaluation of protein α-helix contents

Protein α-helix contents were evaluated through CD experiments. CD experiments were carried out with a Chariscan circular dichroism photomultiplier (Applied Photphsics Limited, UK) equipped with a Quantum Northwest TC125 temperature controller at 25 °C, and protein α-helix contents were calculated by the software CDNN2.1-SimpleSpectra attached to this instrument. The final concentration of proteins in CD measurements was 5 μM in 100 mM Tris-HCl buffer (pH 7.4, 150 mM NaCl). For evaluation of α-helix contents in BSA exposed to urea, 0–8 M urea was added into the BSA-containing buffers and incubated for 40 min at 37 °C prior to measurements.

Molecular docking simulation

The molecular simulation on docking **1** into the three-dimensional structures of different proteins (download from PDB) was carried out by using the program suite AutoDock 4.2.0 (http://www.scripps.edu/mb/olson/doc/autodock). The well used Lamarckian Genetic Algorithm (LGA), an efficient and robust algorithm[41,42] was chosen for the docking calculation. The graphical user interface, AutoDockTools (ADT 1.4.6) was performed to setup each ligand-protein interaction, where all hydrogen atoms were added, Gasteiger charges were calculated and nonpolar hydrogen atoms were merged to carbon atoms. The solvent molecules were removed from the protein three-dimensional structures to obtain the docking grid, and the active site was defined by using AutoGrid. The grid size was set to 60*60*60 points with grid spacing of 0.375 Å, Van der Waals well depth of 0.100 kcal/mol and iteration were set to 200[43] and population size 100. The grid box was centered on the center of the ligand from the corresponding protein structures. Formal structures of the proteins were assigned by the program SYBYL, and the best ranked pose was selected from the ChemScore. The conformation with the lowest binding energy was used to analyze ligand placement.

Cell culture

Human prostate epithelial RWPE 1 cell line, and human HeLa cell line were purchased from China Center for Type Culture Collection, and human prostate cancer DU145 cell line was from Boster Biological Technology, LTD. RWPE 1 cells were grown in keratinocyte-serum free medium (K-SFM, Invitrogen) containing 5 ng/mL human recombinant epithelial growth factor (hEGF, Invitrogen), 0.05 mg/mL bovine pituitary extract (Invitrogen). DU145 cells were cultured in Iscove's modified Dulbecco's medium (IMDM, Invitrogen) supplemented with 10% fetal bovine serum (FBS, Invitrogen). HeLa cells were grown in Dulbecco's modified Eagle medium (DMEM, Invitrogen) containing 10% FBS.

Extraction and quantification of membrane proteins

Extraction of membrane and cytosol proteins from Hela cells was carried by utilization of *Membrane and Cytosol Protein Extraction Kit* (Beyotime Institute of Biotechnology, China). The protein samples were quantified by *BCA Protein Assay Kit* (Beyotime Institute of Biotechnology, China).

Flow cytometry

Fluorescence responses of **1** to expression levels of membrane proteins in living cells were detected by flow cytometry experiments performed with a BD FACSAria III flow cytometer (BD, USA) with an excitation wavelength of 375 nm and hochest-blue filter (450 ± 50 nm). RWPE 1 and DU145 cells were loaded at 37 °C for 1 h with 4 μM **1** in K-SFM and IMDM media, respectively, prior to measurement.

Confocal imaging

All confocal imaging experiments were carried out by a Carl Zeiss laser scanning confocal microscope (Carl Zeiss, Germany). To observe the intracellular **1** localization, RWPE 1 cells were co-stained for 1 h at 37 °C with 4 μM **1** and 40 nm ER-Red (Beyotime institute of biotechnology) in K-SFM. To examine differences in expression of membrane proteins between prostate normal and cancer cells, RWPE 1 and DU145 cells were exposed respectively to 4 μM **1** for 1 h at 37 °C in the corresponding media. Cells were imaged by two-photon excitation at 800 nm for **1**, and single-photon excitation at 561 nm for ER-Red, respectively. The fluorescence signals from 430 to 490 nm for **1** were acquired for imaging with a × 63 (Plan-Apo, NA 1.4, oil immersion) objective. The preparation procedures and imaging for Z-axis scanning samples were the same as those mentioned with a × 100 (EC Plan-Neo, NA 1.3, oil immersion) objective. Data were analyzed by software package attached to this instrument.

Conclusions

In the study presented here, **1** was observed to emit the strong ESIPT fluorescence in the low-polar environments created by protein α-helical regions, and the ESIPT fluorescence intensity was positively correlated with the α-helix content in a protein. The confocal imaging showed that **1** was localized in cell and plasma membranes via the H-bonding interactions with membrane protein α-helices, as indicated by molecular docking simulation. The membrane localization allowed **1** to probe differences in the membrane protein α-helix contents between prostate normal and cancer cells by its changes in the ESIPT emission intensity. The **1**-sensed decrease in the membrane protein α-helix contents should be a consequence of the significant down regulation in expression of zinc transporters in prostate cancer cells. These results revealed that the down regulated expression of the membrane proteins including zinc transporters could become a new biomarker for prostate cancer cell recognition, and **1** could discriminate individual prostate cancer cells by sensing the differences in expression of zinc transporters between prostate normal and cancer cells. Discriminating individual cancer cells from normal cells at molecular levels might underlie the early diagnosis of prostate cancer.

Notes and references

[a] Nan Jiang, Chanli Yang, Xiongwei Dong, Xianglang Sun, Dr. Dan Zhang, Prof. Dr. Changlin Liu
Key Laboratory of Pesticide & Chemical Biology, Ministry of Education, School of Chemistry
Central China Normal University
Chemistry building, Central China Normal University, Wuhan, China
Tel: (+86)-27-67867232.
E-mail: liuchl@mail.ccnu.edu.cn
danzhang@mail.ccnu.edu.cn

† Electronic Supplementary Information (ESI) available: [details of any supplementary information available should be included here]. See DOI: 10.1039/b000000x/

‡ Footnotes should appear here. These might include comments relevant to but not central to the matter under discussion, limited experimental and spectral data, and crystallographic data.

1. P. K. Sengupta, M. Kasha, *Chem. Phys. Lett.*, 1979, **68**, 382.
2. W. H. Chen, Y. Pang, *Tetrahedron Lett.*, 2010, **51**, 1914.
3. A. Sytnik, M. Kasha, *Proc. Natl. Acad. Sci. USA*, 1994, **91**, 8627.
4. A. Sytnik, D. Gormin, *M. Kasha, Proc. Natl. Acad. Sci. USA*, 1994, **91**, 11968.
5. A. Sytnik, J. C. Del Valle, *J. Phys. Chem.*, 1995, **99**, 13028.
6. A. S. Klymchenko, T. Ozturk, V. G. Pivovarenko, A. P. Demchenko, *Tetrahedron Lett.*, 2001, **42**, 7967.
7. S. Ercelen, A. S. Klymchenko, A. P. Demchenko, *FEBS Letters*, 2003, **538**, 25.
8. A. S. Klymchenko, S. V. Avilov, A. P. Demchenko, *Anal. Biochem.*, 2004, **329**, 43.
9. S. V. Avilov, C. Bode, F. G. Tolgyesi, A. S. Klymchenko, J. Fidy, A. P. Demchenko, *Int. J. Biol. Macromol.*, 2005, **36**, 290.
10. F. S. Rodembusch, F. P. Leusin, L. F. Medina, A. Brandelli, V. Stefani, *Photochem. Photobiol. Sci.*, 2005, **4**, 254.
11. R. C. Santos, N. V. S. Faleiro, L. F. Campo, M. L. Scroferneker, V. A. Corbellini, F. S. Rodembusch, V. Stefani, *Tetrahedron Lett.*, 2011, **52**, 3048.
12. T. C. Daboit, C. D. O. Stopiglis, M. Carissimi, V. A. Corbellini, V. Stefani, M. L. Scroferneker, *Mycoses*, 2009, **52**, 507.
13. A. Jäger, V. Stefani, S. S. Guterres, A. R. Pohlmann, *Int. J. Pharm.*, 2007, **338**, 297.
14. M. B. Cardoso, D. Samios, N. P. D. Silveira, Photochem. *Photobiol. Sci.*, 2007, **6**, 99.
15. J. L. Popot, D.M. Engelman, *Annu. Rev. Biochem.*, 2000, **69**, 881.

16. X. A. Zhang, D. Hayes, S. J. Smith, S. Friedle, S. J. Lippard, *J. Am. Chem. Soc.*, 2008, **130**, 15788.
17. S. K. Ghosh, P. Kim, X. A. Zhang, S. H. Yun, A. Moore, S. J Lippard, Z. Medarova, *Cancer Res.*, 2010, **70**, 6119.
18. D. Buccella, J. A. Horowitz, S. J. Lippard, *J. Am. Chem. Soc.*, 2011, **133**, 4101.
19. J. Gumulec, M. Masarík, S. Krízková, P. Babula, R. Hrabec, A. Rovný, M. Masaríková, R. Kizek, *Klin. Onkol.*, 2011, **24**, 249.
20. J. Zou, B. C. Milon, M. M. Desouki, L.C. Costello, R.B. Franklin, *The Prostate*, 2011, **71**, 1518.
21. R. B. Franklin, P. Feng, B. Milon, M. M. Desouki, K.K. Singh, A. Kajdacsy-Balla, O. Bagasra, L. C. Costello, *Mol. Cancer*, 2005, **4**, 32.
22. M. M. Desouki, J. Geradts, B. Milon, R. B. Franklin, L.C. Costello, *Mol. Cancer*, 2007, **6**, 37.
23. M. L. Guerino, *Biochim. Biophys. Acta*, 2000, **1465**, 190.

24. E. Barni, P. Savarino, M. Marzona, M. J. Piva, *Heterocyclic. Chem.*, 1983, **20**, 1517.

25. A. S. Klymchenko, A. P. Demchenko, *Phys. Chem. Chem. Phys.*, 2003, **5**, 461.

26. K. Das, N. Sarkar, D. Majumdar, K. Bhattacharyya, *Chem. Phys. Lett.*, 1992, **198**, 443.

27. S. Tayyab, N. Sharma, M. M. Khan, *Biochem. Biophys. Res. Commun.*, 2000, **277**, 83.

28. B. Ahmad, M. K. A. Khan, S. K. Haq, R. H. Khan, *Biochem. Biophys. Res. Commun.*, 2004, **314**, 166.

29. F. Musiani, E. Arnofi, R. Casadio, S. Ciurli, *J. Biol. Inorg. Chem.*, 2001, **6**, 300.

30. Y. P. Tong, *Acta Cryst.*, 2005, **E61**, o3076.

31. S. Sugio, A. Kashima, S. Mochizuki, M. Noda, K. Kobayashi, *Protein Eng.*, 1999, **12**, 439.

32. J. Yamane, M. Yao, Y. Zhou, Y. Hiramatsu, K. Fujiwara, T. Yamaguchi, H. Yamaguchi, H. Togame, H. Tsujishita, H. Takemoto, I. Tanaka, *J. Appl. Crystallogr.*, 2011, **44**, 798.

33. D. A. Doyle，J. Morais Cabral, R. A. Pfuetzner, A. Kuo, J. M. Gulbis, S. L. Cohen, B.T. Chait, R. MacKinnon, *Science*, 1998, **280**, 69.

34. L. Sun, X. Zeng, C. Yan, X. Sun, X. Gong, Y. Rao, N. Yan, *Nature*, 2012, **490**, 361.

35. E. Granseth, G. Heijne, A. Elofsson, *J. Mol. Biol.*, 2005, **346**, 377.

36. M. Eilers, S. C. Shekar, T. Shieh, S. O. Smith, P. J. Fleming, *Proc. Natl. Acad. Sci. USA*, 2000, **97**, 5796.

37. S. W. Cowan, *Curr. Opin. Struct. Biol.*, 1993, **3**, 501.

38. R. B. Franklin, J. Ma, J. Zou, Z. Guan, B. I. Kukoyi, P. Feng, L. C. Costello, *J. Inorg. Biochem.*, 2003, **96**, 435.

39. L. Aguilar-Bryan, C. G. Nichols, S. W. Wechsler, J. P. Clement, A. E. Boyd, G. Gonzalez, H. Herrera-Sosa, K. Nguy, J. Bryan, D. A. Nelson, *Science*, 1995, **268**, 423.

40. D. E. Gear, J. M. Margaret, R. Efraim, *Biol. Chem.*, 1976, **251**, 6831.

41. G. M. Morris, D. S. Goodsell, R. S. Halliday, R. Huey, W. E. Hart, R. K. Belew, A. J. Olson, *J. Cpmput. Chem.*, 1998, **19**, 1639.

42. N. Brooijmans, I. D. Kuntz, *Annu. Rev. Biophys. Biomol. Struct.*, 2003, **32**, 335.

43. G. M. Morris, D. S. Goodsell, R. Huey, A. J. Olson, *J. Comput. Aide Mol. Des.*, 1996, **10**, 293.
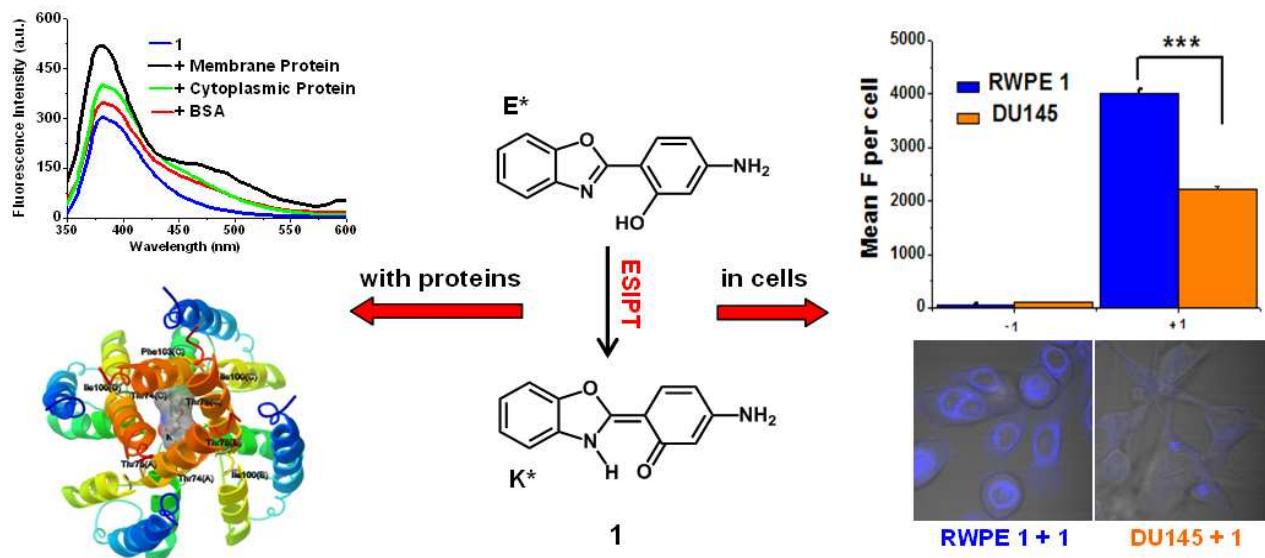
A benzazole derivative, **1**, was observed to take the excited-state intramolecular proton transfer (ESIPT) process with α-helical proteins. The ESIPT fluorescence was positively correlated with the α-helix contents of proteins, and the molecular docking showed that binding sites in α-helical regions had low energy. The cell images showed a difference staining normal and cancer prostate cells by **1**, which might be due to the different membrane protein levels.